Neuron, Vol. 28, 927–939, December, 2000, Copyright ©2000 by Cell Press

Dynamic Control of Presynaptic Ca^{2+} Inflow by Fast-Inactivating K^+ Channels in Hippocampal Mossy Fiber Boutons

Jörg R. P. Geiger and Peter Jonas*
Physiologisches Institut der Universität Freiburg
Hermann-Herder-Str. 7
D-79104 Freiburg
Germany

Summary

Analysis of presynaptic determinants of synaptic strength has been difficult at cortical synapses, mainly due to the lack of direct access to presynaptic elements. Here we report patch-clamp recordings from mossy fiber boutons (MFBs) in rat hippocampal slices. The presynaptic action potential is very short during low-frequency stimulation but is prolonged up to 3-fold during high-frequency stimulation. Voltage-gated K^+ channels in MFBs inactivate rapidly but recover from inactivation very slowly, suggesting that cumulative K^+ channel inactivation mediates activity-dependent spike broadening. Prolongation of the presynaptic voltage waveform leads to an increase in the number of Ca^{2+} ions entering the terminal per action potential and to a consecutive potentiation of evoked excitatory postsynaptic currents at MFB-CA3 pyramidal cell synapses. Thus, inactivation of presynaptic K^+ channels contributes to the control of efficacy of a glutamatergic synapse in the cortex.

Introduction

Current knowledge of the electrical events preceding transmitter release is based on direct recordings from presynaptic elements with highly specialized properties. In the mammalian CNS, recent work has concentrated on glutamatergic calyx synapses in the brainstem (Forsythe, 1994; Borst et al., 1995; Schneggenburger et al., 1999) and GABAergic basket cell terminals in the cerebellum (Southan and Robertson, 1998). Glutamatergic cortical synapses have not been accessible yet due to the smaller diameter of their presynaptic elements. Throughout the cortex, hippocampal mossy fiber boutons (MFBs) are among the largest synaptic terminals. These boutons, presynaptic expansions of granule cell axons, have an average diameter of 3–5 μm and therefore represent candidate structures for presynaptic recording (Blackstad and Kjaerheim, 1961; Amaral and Dent, 1981; Acsády et al., 1998). Furthermore, these boutons are critical stations in the flow of information through the hippocampal trisynaptic circuitry because they represent the primary site of transmission of signals from the dentate gyrus to the CA3 region.

Hippocampal mossy fiber synapses are capable of fast and synchronized transmitter release from several active zones (Brown and Johnston, 1983; Jonas et al., 1993; Geiger et al., 1997) but also show dynamic changes of synaptic strength over a more than 10-fold range (Griffith, 1990; Regehr and Tank, 1991; Johnston et al., 1992; Regehr et al., 1994; Nicoll and Malenka, 1995; Salin et al., 1996). Short-term forms of plasticity, such as paired-pulse facilitation, frequency facilitation, and augmentation (Griffith, 1990; Salin et al., 1996), coexist with long-lasting forms, such as posttetanic potentiation (PTP; Griffith, 1990) and NMDAR-independent long-term potentiation (LTP; Johnston et al., 1992; Nicoll and Malenka, 1995). These forms of plasticity are thought to be expressed mainly presynaptically (Zalutsky and Nicoll, 1990), but the mechanisms and final molecular targets of the modifications (presynaptic ion channels, release machinery, or both) have not been identified.

The shape of the presynaptic action potential is of fundamental importance in determining timing and strength of synaptic transmission (Augustine, 1990; Sabatini and Regehr, 1999). The duration of the presynaptic spike is probably not fixed but may be subject to short- and long-term regulation. In pituitary nerve terminals of the rat, short-term spike broadening (on the timescale of seconds) is induced by high-frequency stimulation and is presumably mediated by K^+ channel inactivation (Jackson et al., 1991). In presynaptic elements of invertebrate neurons, long-lasting spike broadening (on the timescale of minutes or longer) is induced by neuromodulators and is believed to be mediated by K^+ channel modulation (Byrne and Kandel, 1996). Whether dynamic changes in presynaptic spike duration also occur at fast-transmitting synapses in the mammalian CNS remains, however, unclear. Previous studies suggested the presence of inactivating K^+ channel subunits in the mossy fiber termination zone. However, their subcellular location has remained controversial (Sheng et al., 1993; Wang et al., 1994; Rhodes et al., 1997; Cooper et al., 1998). Thus, it is uncertain whether the molecular properties of K^+ channels in hippocampal MFBs are consistent with a possible variation in the duration of the presynaptic spike.

We have developed methods for direct patch-clamp recording from MFBs in acute hippocampal slices. This technical advance allows us to address three fundamental questions of glutamatergic synaptic transmission in the mammalian brain. (1) Which is the time course of the presynaptic voltage signal that triggers vesicular glutamate release? (2) Does the spike shape change under conditions that lead to plastic changes in synaptic strength? (3) If so, what are the mechanisms and functional consequences for transmitter release?

Results

Direct Recording from Hippocampal Mossy Fiber Boutons

Using improved slice techniques and enhanced optical resolution (see Experimental Procedures), we obtained patch-clamp recordings from spherical structures of 3–5 μm diameter in stratum lucidum of acute hippocampal slices (Figure 1). Several morphological characteristics

*To whom correspondence should be addressed (e-mail: jonasp@uni-freiburg.de).

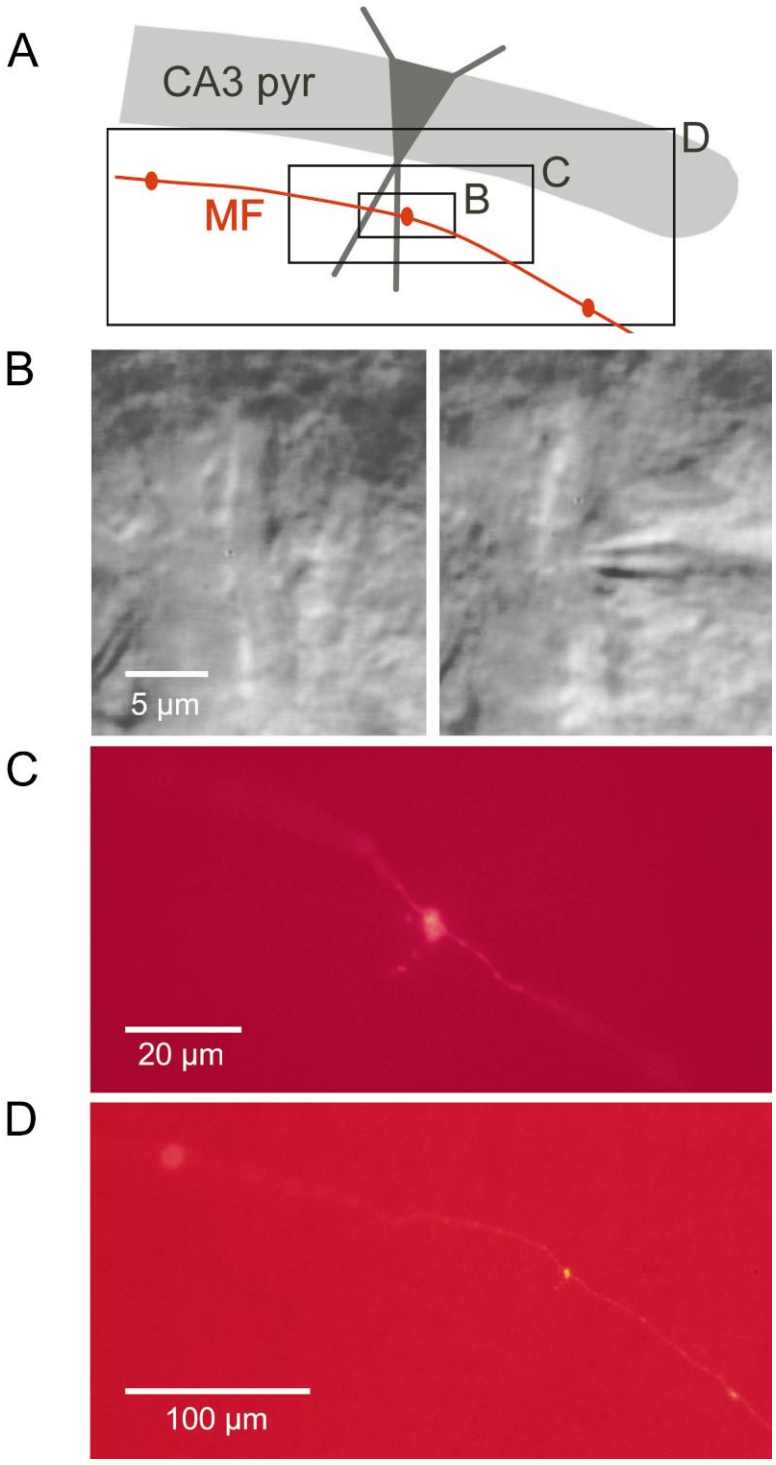

Figure 1. Morphological Identification of MFBs in Hippocampal Slices

(A) Schematic illustration of the CA3 subfield topography, with a CA3 pyramidal neuron in black, the CA3 pyramidal cell layer in gray, and a mossy fiber in red.

(B) IR-DIC photomicrograph of a putative MFB close to the primary apical dendrite of a CA3 pyramidal neuron. Left image before, right image after approach with a patch pipette. Focal plane ~30 μm below the surface of the slice.

(C and D) Epifluorescence photomicrographs of the MFB filled with biocytin and stained using rhodamine-conjugated avidin. Note the staining of mossy fiber axon and adjacent MFBs (D). Also, note filopodial extensions that are characteristic for this type of presynaptic element (Acsády et al., 1998). K-gluconate internal solution.

indicated that these structures were mossy fiber boutons (MFBs), forming en passant synapses on CA3 pyramidal neurons (Blackstad and Kjaerheim, 1961; Amaral and Dent, 1981; Acsády et al., 1998). Intracellular filling with biocytin in the whole-cell configuration labeled both the recorded MFB and an adjacent parent axon (all of 14 MFBs stained; Figure 1C). The axon ran tangentially through stratum lucidum and showed several regularly spaced expansions, most likely adjacent MFBs (Figure 1D; Amaral and Dent, 1981). In 12 MFBs filled with biocytin, the axon was cut in the hilar region; in 2 MFBs, however, the granule cell soma from which the axon originated was also labeled. MFBs showed several filopodial extensions, as thought to be characteristic of this particular type of synaptic terminal (Acsády et al., 1998). These results indicate that it is possible to identify MFBs in brain slices reliably and to record from them selectively.

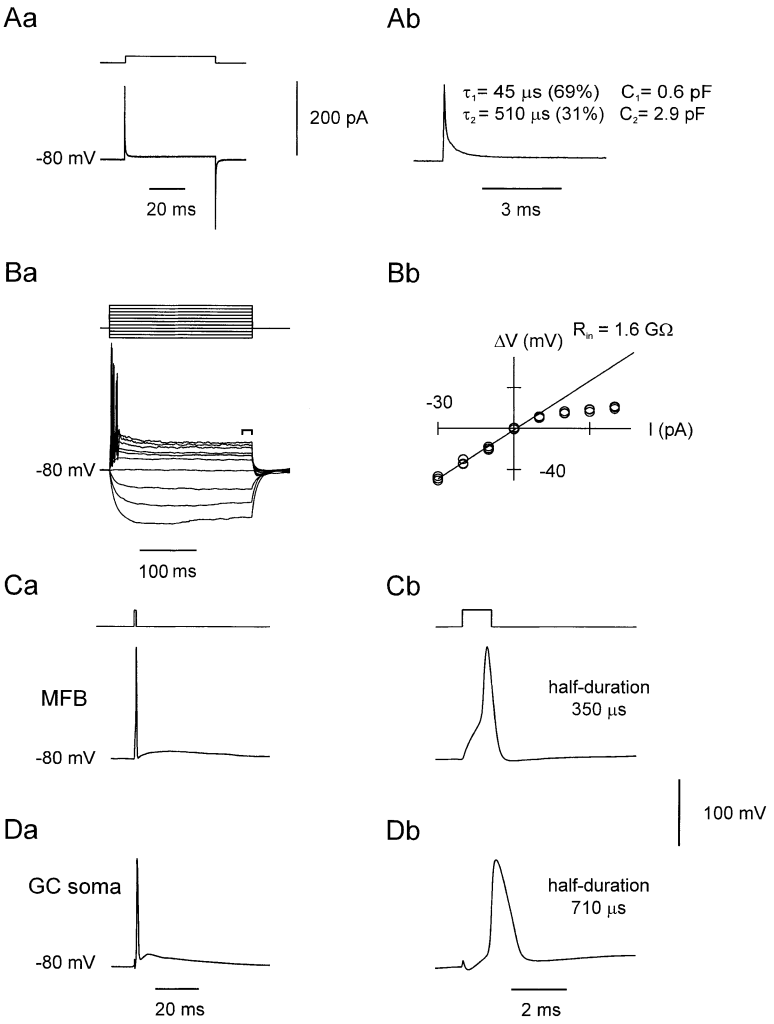

Figure 2. Electrical Properties of MFBs as Revealed by Direct Patch-Clamp Recording

(A) Capacitive and leak currents in a whole-cell recorded MFB (test pulse amplitude ΔV = 10 mV). The decay of the capacitive transient was fitted with the sum of two exponentials, with time constants (τ), amplitude contributions (A), and corresponding capacitances [$C = (A\tau)/\Delta V$]. Assuming a specific capacitance of 1 $\mu F\ cm^{-2}$, the fast component corresponds to a sphere with 4.4 μm diameter, in agreement with the physical diameter of this MFB (4–6 μm).

(Ba) Voltage responses of the whole-cell recorded MFB to 250 ms hyper- or depolarizing current pulses (−30 to 70 pA, 10 pA increment). The 40 and 50 pA pulses evoked 1 spike per trace, 60 pA pulses 2 spikes, and 70 pA pulses 3 spikes.

(Bb) Voltage-current relation; the current was measured at the end of the 250 ms current pulse (see bracket above traces in Ba). The line corresponds to linear regression of data points from −30 to 0 pA. Note the marked rectification, which indicates subthreshold activation of voltage-gated K^+ channels.

(C and D) Action potentials in a whole-cell recorded MFB (C) and in a granule cell soma (D) evoked by 1 ms current pulses (200 pA and 1 nA, respectively) shown at different time bases.

Traces in (A)–(C) are from the same MFB shown in Figure 1. K-gluconate internal solution. Recording temperature 34°C.

The Shape of the Presynaptic Voltage Signal that Triggers Glutamate Release

Recording from MFBs allowed us to examine the electrical properties of a cortical presynaptic element (Figure 2). Capacitive currents in the whole-cell voltage-clamp configuration decayed biexponentially, with a major fast component (1.22 ± 0.13 pF), probably corresponding to the charging of the terminal, and a minor slow component (2.95 ± 0.30 pF, 12 MFBs), presumably representing the charging of the axon (10 mV pulses; Figure 2A). Long depolarizing current pulses in the current-clamp configuration evoked single action potentials or bursts of up to three action potentials in MFBs (Figure 2B). The voltage-current relationship at the end of the 250 ms current pulse was markedly rectifying, with a region of high input resistance (>1 GΩ) below the resting potential (Figure 2B). Action potentials evoked by 1 ms current pulses were brief (half-duration 379 ± 8 μs, range: 254–533 μs; 59 MFBs; 34°C) and overshooting (amplitude 114.9 ± 1.2 mV, measured from holding potential), and were followed by a brief afterhyperpolarization and a long-lasting afterdepolarization (amplitude 6.9 ± 0.6 mV; half-duration 36.2 ± 2.7 ms; 38 MFBs; Figure 2C). The properties of presynaptic spikes were very different from those of action potentials in granule cell somata, which had a significantly longer half-duration (678 ± 45 μs, range: 507–903 μs; 9 somatic granule cell recordings; $P < 0.001$) and were followed by a more pronounced afterdepolarization (20.1 ± 2.7 mV; $P < 0.002$; Figure 2D). These results indicate that the shape of the presynaptic action potential differs markedly from that recorded in the somatic compartment of the same neuron.

Activity-Dependent Broadening of Presynaptic Action Potentials

Granule cells in the hippocampal network in vivo generate high-frequency trains of action potentials in specific behavioral contexts (Jung and McNaughton, 1993; Skaggs et al., 1996; Wiebe and Stäubli, 1999). We therefore examined the shape of action potentials in MFBs evoked by brief depolarizing current stimuli at frequencies of 10–100 Hz (Figure 3). During high-frequency trains, the duration of the presynaptic spike became substantially longer (Figure 3B), which was mainly due to a decrease in the rate of repolarization. For 50 Hz trains, the initial prolongation was 1.3% per action potential, and the maximal broadening was 206% (Figure 3C; 10 MFBs). The dynamic properties of presynaptic spikes differed from those in granule cell somata, where the extent of broadening was much smaller in the fre-

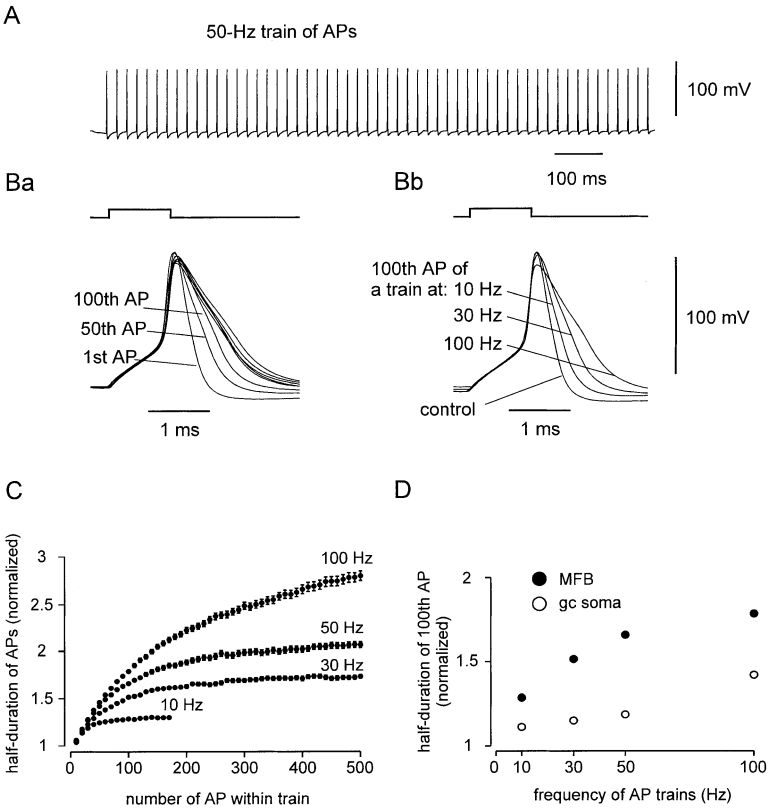

Figure 3. Onset of Activity-Dependent Broadening of Presynaptic Action Potentials in MFBs

(A) Train of action potentials evoked at a frequency of 50 Hz. One millisecond pulses (300 pA).

(Ba) Every fiftieth action potential is shown superimposed with the first action potential in the train.

(Bb) The hundredth action potentials in 10, 30, and 100 Hz trains are superimposed with the first action potential in the 50 Hz train. KCl internal solution.

(C) Plot of duration of action potentials at half-maximal amplitude in whole-cell recorded MFBs against the number of the action potential within the train for the frequencies indicated. Data points were normalized to the half-duration of the first action potential and were condensed with 10 values per point.

(D) Plot of the increase in half-duration after 100 action potentials in MFBs (filled circles) and GC somata (open circles), plotted against stimulation frequency.

Data points in (C) and (D) are means from 9–10 MFBs and 8 granule cell somatic recordings. KCl or K-methylsulfate internal solution.

quency range examined (Figure 3D). Thus, high-frequency stimulation over seconds leads to robust and specific prolongation of the presynaptic spike.

High-frequency activity in granule cells in vivo often occurs in a patterned manner, dependent on environmental cues (Jung and McNaughton, 1993; Wiebe and Stäubli, 1999) and endogenous theta rhythm (Skaggs et al., 1996). We therefore examined whether activity-dependent spike broadening was long lasting and whether it was induced by naturally occurring patterns of activity (Figure 4). After a 1 s train of stimuli at 100 Hz followed by a 1 s period of recovery, the action potential was prolonged to 127% ± 5% of the control value (Figures 4A and 4B; 5 MFBs). Furthermore, a theta-burst stimulation paradigm (Skaggs et al., 1996), with 200 Hz trains of 6 action potentials applied at a frequency of 5 Hz (corresponding to an average stimulation frequency of 30 Hz), resulted in a substantial cumulative action potential broadening (Figures 4C and 4D; 5 MFBs). The extent of broadening was 131% ± 3% after 3 bursts and 148 ± 4% after 6 bursts. Thus, action potential broadening induced by high-frequency stimulation lasts several seconds and is likely to occur under physiological conditions.

Gating and Molecular Identity of Presynaptic K^+ Channels

The selective decrease in the rate of repolarization suggests an involvement of K^+ channels in activity-dependent spike broadening, as proposed for invertebrate neurons (Aldrich et al., 1979; Quattrocki et al., 1994; Ma and Koester, 1996). We examined this possibility in outside-out patches isolated from MFBs (Figure 5). This approach allowed us to study presynaptic channels in isolation and avoided problems of insufficient voltage-clamp and ion accumulation or depletion.

K^+ channels in outside-out patches isolated from MFBs showed a negative activation threshold and a fast onset of inactivation. The midpoint potential of the activation curve was −26 mV (Figures 5A and 5C; 10 patches). The time constant of inactivation onset during 100 ms pulses was 15.5 ± 0.6 ms (range: 6.2–41.0 ms), and the percentage of current remaining at the end of the 100 ms pulse was 26.7% ± 0.9% (range: 16%–52%; 30 mV test pulse potential; 75 patches). Inactivation was also induced by long prepulses; the midpoint potential of the inactivation curve was −72 mV (Figures 5B and 5C). In contrast to the fast onset of inactivation, recovery of presynaptic K^+ channels from inactivation induced by 100 ms pulses was slow; the time constant of the dominating component in MFB outside-out patches was 497 ms (−120 mV interpulse potential; Figures 5D and 5E; 4–6 patches per point). Accordingly, repetitive activation of presynaptic K^+ channels by 3 ms pulses induced cumulative inactivation (Figure 5F), suggesting that K^+ channel inactivation is the major mechanism underlying spike broadening.

The specific functional properties of presynaptic K^+ channels raise the question of their molecular identity. We therefore examined the effects of the K^+ channel blockers tetraethylammonium (TEA) and α-dendrotoxin (DTX; Figure 6), which blocks selectively Kv1 channels (Jonas et al., 1989; Stühmer et al., 1989). K^+ currents in presynaptic outside-out patches were ~50% blocked

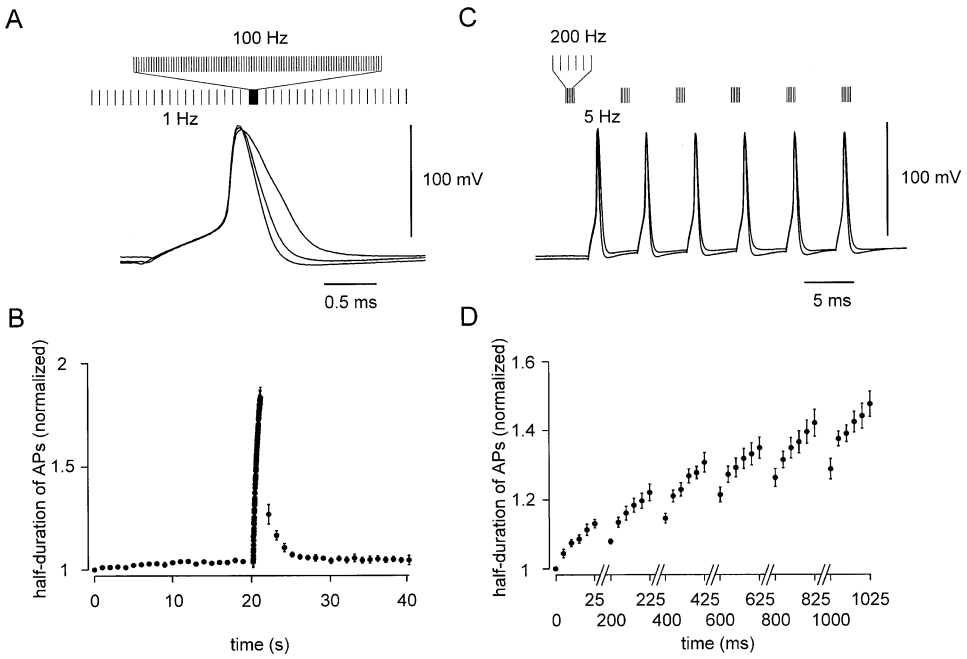

Figure 4. Recovery from Spike Broadening and Cumulative Broadening during Bursts

(A) Action potential broadening in whole-cell recorded MFBs during 100 Hz stimulation (inset). First action potential in the control period, last action potential in the 100 Hz epoch, and first action potential in the recovery period are shown superimposed.

(B) Plot of duration of action potentials at half-maximal amplitude against time before, during, and after 100 Hz stimulation. Values were normalized to the half-duration of the first action potential. Note the slight gradual increase of the half-duration after onset of the 1 Hz stimulation at time 0.

(C) Action potential broadening during theta-burst stimulation in another MFB. The 100 Hz trains of 6 action potentials were applied at a frequency of 5 Hz (inset, corresponding to an average frequency of 30 Hz). Action potentials during the first and the last train are shown superimposed.

(D) Plot of half-duration of action potentials against time during the theta-burst protocol. Half-durations were measured from the baseline preceding the first stimulus in each train and were normalized to the half-duration of the first action potential.

Pulse duration 1 ms, pulse intensity 200–300 pA. Data points in (B) and (D) are means from 5 MFBs. KCl internal solution.

by 1 mM TEA (Figure 6A) and 1 μM DTX (Figure 6C), and ~80% inhibited by 10 mM TEA (Figure 6B), with almost indistinguishable effects on the peak current and the current at the end of the 100 ms pulse (Figure 6D; 18 patches total). A comparison of native K^+ channels in MFBs with recombinant channels expressed in host cells (Chandy and Gutman, 1995) suggests that inactivation could be conferred by either Kv1.4 α subunits (Ruppersberg et al., 1990) or auxiliary β subunits (Rettig et al., 1994). Likewise, TEA sensitivity could be conferred by Kv1.1, 1.3, and 1.6 subunits, while DTX sensitivity could be generated by Kv1.1, 1.2, and 1.6 subunits (Stühmer et al., 1989). However, Kv1.6 subunits have an N-type inactivation-preventing (NIP) domain (Roeper et al., 1998). Thus, the functional properties of native channels in MFBs are most consistent with Kv1.1/Kv1.4 heteromers or with Kv1.1 α subunit/β subunit combinations (Rhodes et al., 1997).

Action Potential Broadening Increases Presynaptic Ca^{2+} Inflow

The effects of K^+ channel–regulated action potential broadening on presynaptic Ca^{2+} currents and transmitter release are difficult to predict (Llinás et al., 1981; Spencer et al., 1989; Augustine, 1990). To determine the quantitative relationship between spike duration and amplitude and shape of the presynaptic Ca^{2+} current that triggers release, mock action potential waveforms (Wheeler et al., 1996) were applied to MFBs in the whole-cell voltage-clamp configuration, and their duration was varied systematically in a plausible range (Figure 7). Ca^{2+} currents were isolated pharmacologically using 1 μM TTX and 20 mM TEA in the external solution and Cs^+ in the internal solution. Currents evoked by depolarizing stimuli in these conditions were blocked (>95%) by 1 mM Cd^{2+}, confirming that they were mediated entirely by voltage-gated Ca^{2+} channels.

Short mock action potentials with a half-duration of 350 μs activated a transient Ca^{2+} current with a peak amplitude of 503 ± 38 pA and a half-duration of 173 ± 8 μs (Figure 7A; 6 MFBs). Similarly, action potentials recorded previously from a different MFB (half-duration 360 μs), when applied as voltage-clamp commands, evoked a Ca^{2+} current with a peak amplitude of 460 ± 109 pA and a half-duration of 167 ± 2 μs (Figure 7B; 4 MFBs). With both waveforms, the Ca^{2+} current onset coincided approximately with the peak of the action potential, whereas the maximum occurred in the repolarization phase.

With both mock action potentials (Figure 7A) and realistic action potentials (Figure 7B), broadening of the action potential waveform resulted in an increase in half-

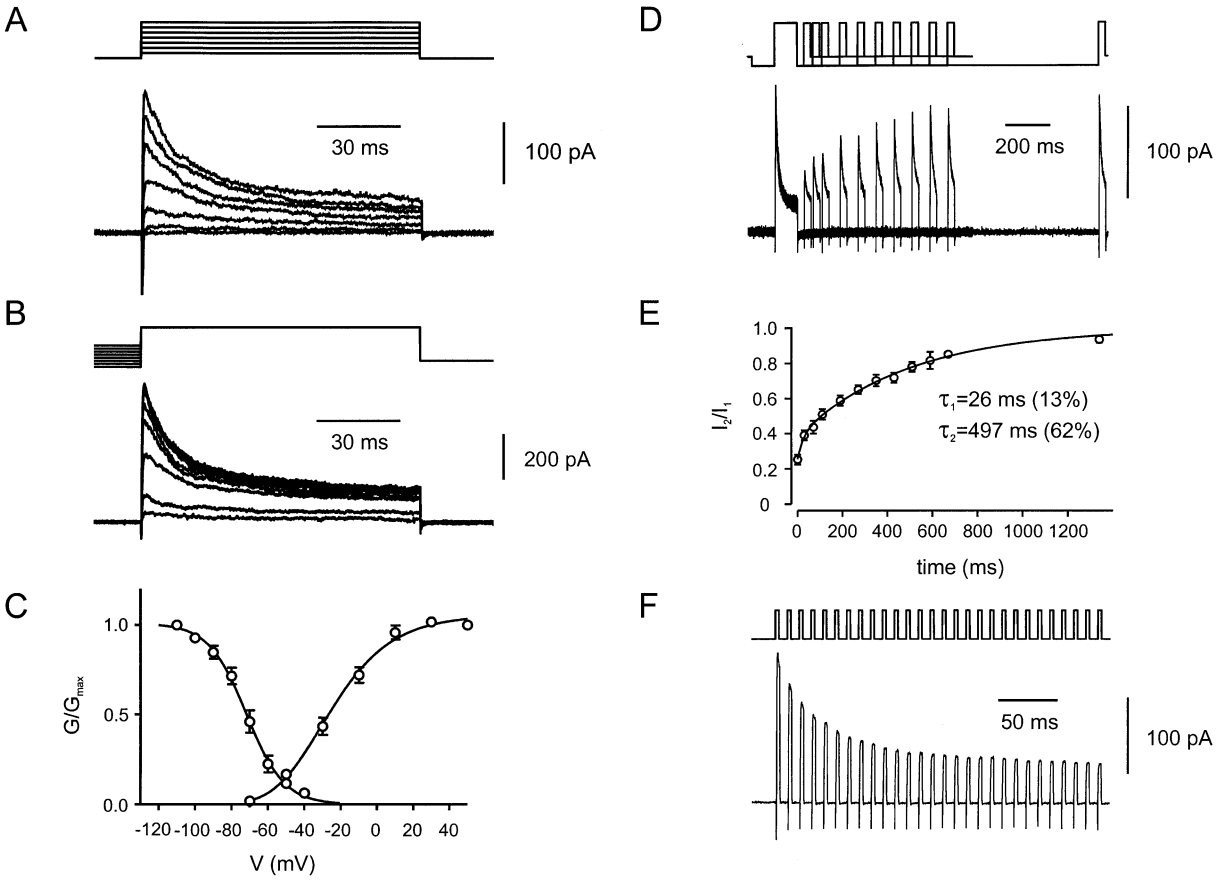

Figure 5. Activation and Inactivation of Voltage-Gated K^+ Channels in MFBs

(A) K^+ currents activated in a MFB outside-out patch by test pulses between −70 and +50 mV (20 mV steps).

(B) Currents activated in a MFB outside-out patch by test pulses to +20 mV, preceded by 10 s prepulses between −110 and −40 mV (10 mV steps).

(C) Activation and steady-state inactivation curves. Ratio of measured and maximal conductance (G/G_{max}), plotted against testpulse and prepulse potential, respectively. Activation data were fitted with a Boltzmann function raised to the fourth power, inactivation data with a simple Boltzmann function. For the activation curve, the midpoint potential was −26 mV (corresponding to $G/G_{max} = 0.5$) and the slope factor 20.7 mV. For the inactivation curve, the midpoint potential was −72 mV and the slope factor 9.6 mV. Data from 10 and 8 patches, respectively.

(D) Recovery of presynaptic K^+ channels from inactivation. Pulse protocol: 100 ms prepulse to −120 mV, 100 ms conditioning pulse to +20 mV, pulse of variable duration to −120 mV, 30 ms test pulse to +20 mV, and step back to −90 mV.

(E) Amplitude of the peak current evoked by the test pulse, divided by that evoked by the conditioning pulse, plotted against interpulse interval. Data points represent means from 4–6 patches. Data points were fitted with the sum of two exponentials; time constants and amplitude contributions as indicated.

(F) Cumulative inactivation of K^+ channels induced by repetitive activation. Traces are K^+ currents activated by a series of pulses to +20 mV (3 ms duration; 7 ms interpulse interval). Holding potential and potential between pulses −90 mV.

Traces shown were corrected for leak and capacitive currents using a P/−4 method and represent averages of 3 (A), 2 (B), 3 (D), and 10 (F) single sweeps. Transient inward Na^+ currents at the beginning of the test pulse are also visible. KCl internal solution.

duration, a decrease in the peak amplitude, and an increase in the integral of the presynaptic Ca^{2+} current. For the mock action potentials, an increase in half-duration to 129% (from 350 to 450 μs) increased the half-duration of the Ca^{2+} current to 140%, decreased the peak amplitude to 92%, and increased the Ca^{2+} inflow to 130% (Figures 7A and 7C; 6 MFBs). For the realistic action potentials, an increase in half-duration to 133% increased the half-duration of the Ca^{2+} current to 143%, decreased the peak amplitude to 90%, and increased the Ca^{2+} inflow to 127% (Figures 7B and 7C; 4 MFBs). These results indicate that action potential broadening leads to a proportional increase in the number of Ca^{2+} ions entering the presynaptic terminal per spike.

Effects of Changes in Presynaptic Action Potential Duration on Glutamate Release

To address the effects of action potential broadening on strength and timing of quantal transmitter release, we made simultaneous recordings from presynaptic MFBs and postsynaptic CA3 pyramidal neurons (Figure 8). We first examined EPSCs evoked by presynaptic action potentials in the current-clamp configuration (Figure 8A). Under these conditions, the mean value of the synaptic delay measured from the steepest point in the rising phase of the presynaptic action potential to the onset of the average EPSC was 713 ± 28 μs (7 pairs).

To examine the consequences of spike broadening for synaptic strength and delay, we applied action po-

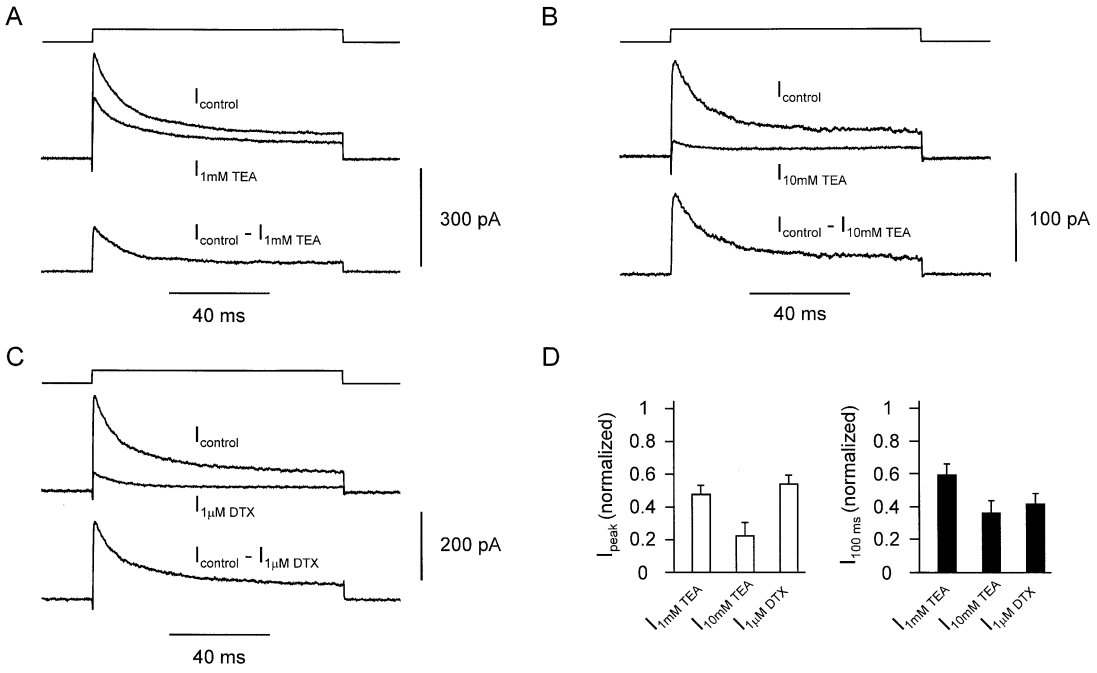

Figure 6. Pharmacological Evidence for the Expression of Inactivating Kv1 Channels in MFBs

(A and B) K^+ currents activated by 100 ms pulses to +30 mV in the absence ($I_{control}$) and presence of 1 mM (A, $I_{1\ mM\ TEA}$) or 10 mM TEA (B, $I_{10\ mM\ TEA}$).

(C) Currents activated by 100 ms pulses to +30 mV in the absence ($I_{control}$) and in the presence of 1 μM DTX ($I_{1\ \mu M\ DTX}$).

The bottom trace represents the blocked current component obtained by digital subtraction. Traces shown represent averages of 6–28 single sweeps. Effects of TEA, and to some extent of DTX, were reversible (not illustrated).

(D) Bar graph summarizing the effects of the K^+ channel blockers. Open bars, normalized peak current; filled bars, normalized current at the end of the 100 ms pulse, both in the presence of blockers. Data from 5, 3, and 12 patches, respectively. KCl internal solution.

tentials as voltage-clamp commands at low frequency (0.13 Hz) in the presence of 1 μM TTX and 20 mM TEA and simultaneously recorded both presynaptic Ca^{2+} currents and postsynaptic EPSCs (Figures 8B–8D; 4 pairs). Broadening of the presynaptic action potentials to 133% increased the EPSC amplitude to 171% ± 26% (Figure 8D), while the synaptic delay increased slightly (from 670 ± 27 μs to 777 ± 38 μs). These results indicate that action potential broadening leads to an enhancement of synaptic strength at the mossy fiber-CA3 pyramidal cell synapse under certain conditions.

Discussion

The Mossy Fiber Bouton: A Model for Presynaptic Recording in the Cortex

Improved patch-clamp techniques in brain slices have allowed us to record from hippocampal MFBs. Passive and active electrical properties, particularly small capacitance, large input resistance, and the ability to generate action potentials allow a reliable identification during the experiment. These properties distinguish MFBs from glial cells, which have much smaller input resistance and express few, if any, voltage-gated Na^+ channels (Steinhäuser, 1993). The properties are also very different from those of CA3 pyramidal neuron dendrites (Spruston et al., 1995) and interneurons in the stratum lucidum (Spruston et al., 1997), which both have a much larger capacitance due to their greater surface membrane areas. Finally, the morphological properties (Figure 1) and the capability to release glutamate onto postsynaptic CA3 pyramidal neurons (Figure 8) identify MFBs unequivocally.

In comparison to other presynaptic structures in the mammalian nervous system from which recordings were obtained (Jackson et al., 1991; Stanley, 1991; Thorn et al., 1991; Forsythe, 1994; von Gersdorff and Matthews, 1994; Borst et al., 1995; Bischofberger and Jonas, 1997; Forsythe et al., 1998; Schneggenburger et al., 1999), the MFB has several technical advantages. Fast EPSCs in the target neurons can be examined directly as a real-time assay of the release process. This is not possible in hypophyseal nerve terminals, which secrete peptides into the circulation (Jackson et al., 1991; Thorn et al., 1991). Adequate presynaptic voltage-clamp can be established in the MFB at physiological temperatures (e.g., Figures 7 and 8), due to electrotonic compactness and small capacitance (1 pF versus versus 23 pF at calyces with short preterminal axons; Borst and Sakmann, 1999). However, a limitation of the MFB recording technique at the present stage is the instability of release (see Experimental Procedures). Thus, analysis of long-term aspects of synaptic transmission will require presynaptic perforated patch recording.

Activity-Dependent Broadening of the Presynaptic Spike

Unlike previous attempts using field potential recording or voltage-sensitive dyes, the present approach allows

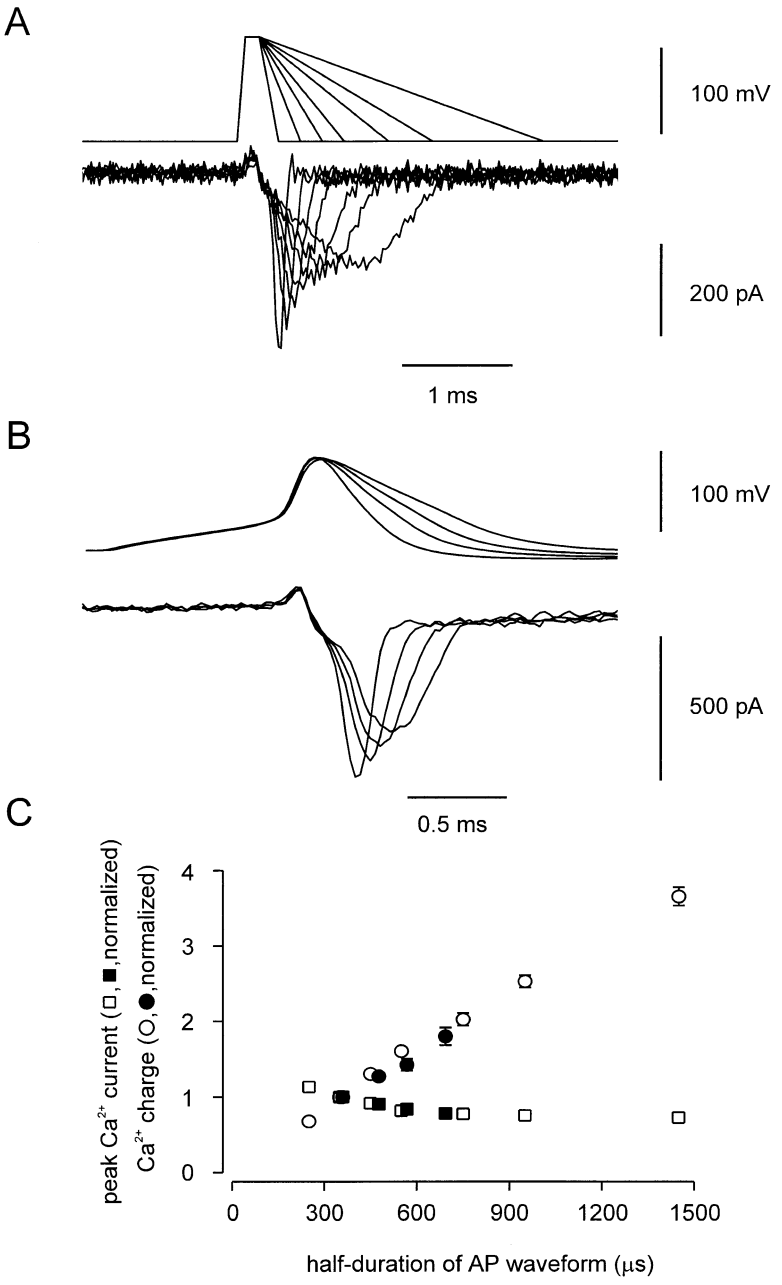

Figure 7. Action Potential Broadening in MFBs Increases Presynaptic Ca^{2+} Inflow

(A and B) Voltage-clamp commands (upper traces) and corresponding Ca^{2+} currents (lower traces) in whole-cell recorded MFBs. Traces shown were corrected for leak and capacitive currents using a P/−4 method. The bath solution contained 1 μM TTX and 20 mM TEA to block voltage-gated Na^+ and K^+ channels. Voltage protocol: mock action potentials in (A) (holding potential −80 mV, 75 μs ramp to +40 mV, 125 μs at +40 mV, and ramp of variable duration back to −80 mV) and realistic action potentials in (B) (action potential 1, 25, 50, and 100 in a 50 Hz train, with half-durations of 360, 477, 568, and 693 μs, respectively, recorded previously from a different MFB, i.e., the same MFB as illustrated in Figures 3A and 3B).

(C) Peak current amplitude (squares) and integral (circles; determined in a 5 ms time window), plotted against half-duration of the voltage-clamp command. Open symbols indicate values for mock action potentials, filled symbols represent realistic action potentials. Values were normalized to the values for the mock action potentials and realistic action potentials with half-durations of 350 μs and 360 μs, respectively. For the shortest mock action potential (250 μs), the mean absolute values were: half-duration 108 ± 4 μs, peak amplitude 574 ± 50 pA, and charge 81 ± 12 fC. For the shortest realistic action potential (360 μs), absolute values were: half-duration 167 ± 2 μs, peak amplitude 460 ± 109 pA, and charge 122 ± 22 fC. Filter frequency 20 kHz. Data from 6 and 4 MFBs, respectively. CsCl internal solution.

us to examine absolute voltages in individual presynaptic elements directly at the sites of transmitter release. We find that the presynaptic spike in MFBs is markedly shorter (mean half-duration 380 μs) than that in granule cell somata (680 μs). Furthermore, the presynaptic voltage returns to the resting value relatively directly, whereas the somatic spike is followed by a larger afterdepolarization (Figures 2C and 2D). Thus, the presynaptic action potential in MFBs during low-frequency stimulation is a brief pulse-like event, comparable to that at the calyx of Held (half-duration 260 μs; Borst et al., 1995; 36°C).

During repetitive stimulation (>10 Hz), action potentials in MFBs show marked activity-dependent broadening (Figures 3 and 4). Two independent lines of evidence suggest that this broadening is physiologically significant. First, granule cells in vivo generate spikes with frequencies of 10–50 Hz in certain behavioral contexts, for example, in place field centers (Jung and McNaughton, 1993; Skaggs et al., 1996) and during odor-guided tasks (Wiebe and Stäubli, 1999). Second, the optimal stimulation frequency range to induce LTP at the mossy fiber-CA3 pyramidal cell synapse in vivo is 10–50 Hz (Yeckel and Berger, 1998). In contrast to presynaptic action potentials in MFBs, spikes in granule cell somata show very little broadening in this frequency range. This indicates that spike broadening is a specific property of the presynaptic element. Furthermore, unlike presynaptic action potentials in the MFB, spikes at the calyx of Held have a virtually constant duration during repetitive

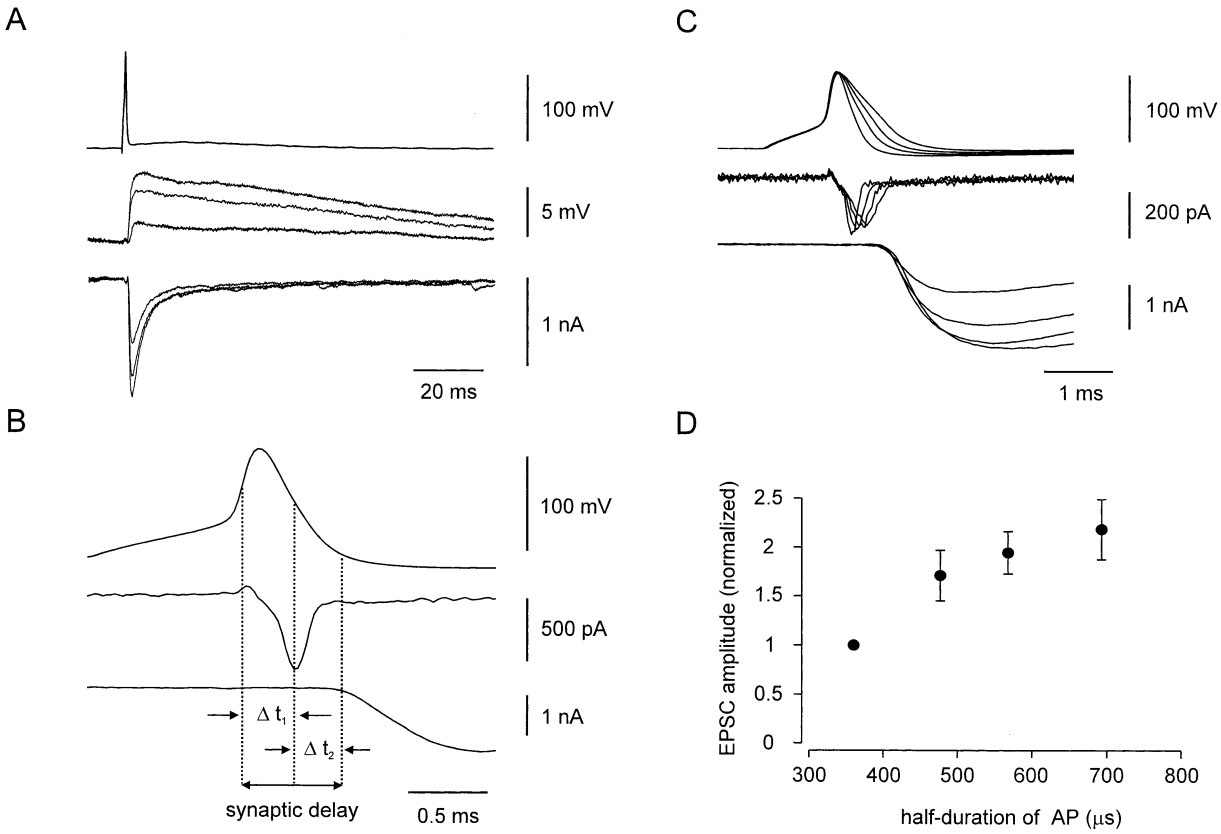

Figure 8. Action Potential Broadening Potentiates Transmitter Release

(A) Simultaneous whole-cell recording from a presynaptic MFB and a postsynaptic CA3 pyramidal neuron. Upper trace, presynaptic action potential recorded in the MFB in the current-clamp configuration; middle and bottom traces, single EPSPs and EPSCs (nonconsecutive) recorded in the CA3 pyramidal neuron. Synaptic delay was 676 μs in this experiment. Holding potential −70 mV (pre- and postsynaptically), K-methylsulfate (presynaptic) and K-gluconate (postsynaptic) internal solutions. Recording temperature 34°C.

(B) Timing of presynaptic action potential, Ca^{2+} current, and transmitter release. Simultaneous recording from a MFB and a postsynaptic CA3 neuron. Action potential applied as a voltage-clamp command (top), presynaptic Ca^{2+} current (center, corrected for leak and capacitive current), and EPSC (bottom) are depicted. Dotted vertical lines indicate the maximum of the first derivative of the presynaptic action potential, the maximum of the presynaptic Ca^{2+} current, and the onset of the EPSC, respectively (with time differences $\Delta t_1 = 313$ μs and $\Delta t_2 = 306$ μs). Ca^{2+} currents (filtered at 20 kHz) and EPSCs are means from 2 runs. Same MFB as that shown in Figure 7B. Recording temperature 35°C.

(C) Potentiation of release by action-potential broadening. Presynaptic action potential waveforms of increasing duration (action potential 1, 25, 50, and 100 in a 50 Hz train recorded previously from a different MFB, i.e., the same MFB illustrated in Figures 3A and 3B), presynaptic Ca^{2+} currents (center), and EPSCs (bottom, largest EPSC corresponding to the broadest presynaptic spike). Different pair from that shown in (B). Ca^{2+} currents (filtered at 20 kHz) and EPSCs are means from 5 runs.

(D) Plot of EPSC amplitude against half-duration of the action potential command voltage. Data are shown normalized to the amplitude of the EPSC evoked by the shortest presynaptic waveform. Data from four pairs; same experiments as shown in Figure 7C (filled symbols). CsCl (presynaptic) and K-methylsulfate (postsynaptic) internal solutions.

stimulation (Wang and Kaczmarek, 1998; Borst and Sakmann, 1999). This suggests that spike broadening operates specifically at synapses with dynamic transmission properties. Thus, spike broadening in MFBs is expressed selectively and appears to be relevant in certain behavioral contexts.

K^+ Channel Inactivation as the Molecular Mechanism Underlying Spike Broadening

Our results indicate that inactivating, DTX-sensitive K^+ channels (presumably assembled from Kv1.1 α/1.4 α or Kv1.1 α/β subunits; Chandy and Gutman, 1995) are the main molecular determinants of activity-dependent spike broadening. The conclusion that presynaptic K^+ channels in MFBs are primarily assembled from Kv1 subunits is consistent with the effects of DTX on both the amplitude of compound mossy fiber EPSCs (10-fold potentiation by bath application of 200 nM DTX; Simmons and Chavkin, 1996) and the duration of presynaptic action potentials in MFBs (140%–249% broadening by focal application of 1 μM DTX, 4 MFBs, unpublished data).

The expression of functionally and molecularly distinct K^+ channels confers several specific electrical properties to MFBs. First, the low threshold for activation and deactivation of presynaptic K^+ channels (approximately −60 mV) ensures rapid and complete reset of the membrane potential after a spike. Second, the combination of fast inactivation onset and slow inactivation recovery in MFBs generates cumulative inactivation of K^+ channels during repetitive stimulation, which underlies spike broadening (Ma and Koester, 1996). Thus,

these channels implement a "molecular memory" operating on the timescale of seconds. Third, the presence of steady-state inactivation close to the resting potential suggests the possibility that ionotropic receptors in MFBs may regulate transmitter release by depolarization and subsequent K^+ channel inactivation (Schmitz et al., 2000). Finally, the tentative identification of presynaptic K^+ channels as Kv1 members suggests that they could be targets of long-lasting modification. In Shaker K^+ channels, the *Drosophila* homologs of Kv1, phosphorylation by the catalytic subunit of protein kinase A promotes inactivation, whereas dephosphorylation reduces inactivation (Drain et al., 1994). A similar modulation may occur in hippocampal MFBs, where neuromodulator effects (e.g., norepinephrine; Hopkins and Johnston, 1984) and long-term changes in synaptic strength (Weisskopf et al., 1994) converge on the cAMP protein kinase A pathway.

The Impact of Action Potential Shape on Ca^{2+} Inflow and Glutamate Release

During action potential broadening, the peak amplitude of the Ca^{2+} current is reduced, but the total charge per spike increases (Figure 7). The reduction in the amplitude may be due to both decrease of the driving force for Ca^{2+} inflow and partial deactivation of Ca^{2+} channels before the peak is reached. Independently, the total Ca^{2+} charge increases, because deactivation of Ca^{2+} channels proceeds more slowly as the rate of repolarization is reduced (see J. Bischofberger et al., 1999, Soc. Neurosci., abstract). Action potential broadening potentiates the amplitude of the EPSC (Figures 8C and 8D), implying that the integral rather than the maximum value of the Ca^{2+} current determines the release probability (Borst and Sakmann, 1999). A prolongation of the presynaptic voltage waveform by 33% augments the Ca^{2+} charge by 27%, which in turn increases the EPSC peak amplitude by 71%. This suggests a power relationship between Ca^{2+} charge and EPSC at the MFB-CA3 pyramidal neuron synapse, with an apparent Hill coefficient of >2. Although these results were obtained with low-frequency stimulation, they suggest that action potential broadening contributes to an enhancement of presynaptic Ca^{2+} inflow and glutamate release under dynamic conditions.

The Impact of Action Potential Broadening on Dynamics and Plasticity

How does action potential broadening contribute to the regulation of synaptic strength at the mossy fiber synapse? A major contribution of spike broadening to frequency facilitation is somewhat unlikely, given that the frequency window is >10 Hz for action potential broadening at 34°C (this paper) but <5 Hz for frequency facilitation at room temperature (Regehr et al., 1994; Salin et al., 1996). In contrast, a direct contribution of spike broadening to augmentation following high-frequency (e.g., 100 Hz) stimulation is highly plausible, since both the recovery from spike broadening and the decay of augmentation occur on the timescale of seconds (Griffith, 1990). With behaviorally relevant activity patterns, such as theta-burst activity, cumulative spike broadening may induce cumulative augmentation of synaptic transmission.

Spike broadening will further boost the induction of PTP and LTP indirectly by enhancement of presynaptic Ca^{2+} inflow during high-frequency stimulation (Regehr and Tank, 1991; Regehr et al., 1994) and consecutive activation of Ca^{2+}-dependent signaling cascades (Villacres et al., 1998). Additionally, spike broadening may enable the release of opioid peptides from large dense-core vesicles, which require global increases in presynaptic Ca^{2+} concentration for fusion (Verhage et al., 1991). Neuropeptide corelease, in turn, is expected to modulate mossy fiber plasticity (e.g., Derrick and Martinez, 1994).

In conclusion, we have established a novel preparation for recording from presynaptic elements at a cortical synapse. We have found activity-dependent broadening of presynaptic action potentials, and we have identified inactivation of voltage-gated K^+ channels as the underlying molecular mechanism. Furthermore, we have addressed possible consequences for presynaptic Ca^{2+} entry and transmitter release. Thus, our results emphasize the importance of electrical events in the dynamic regulation of synaptic strength.

Experimental Procedures

Slice Preparation and Visual Identification of MFBs

Twenty- to twenty-eight-day-old Wistar rats were killed by decapitation, in accordance with institutional guidelines. Transverse hippocampal slices (250–300 μm thickness) were cut in ice-cold sucrose-containing physiological saline using vibratomes (DTK-1000, Dosaka, Kyoto, Japan or a homemade slicer). Both vibratome constructions minimized vertical vibrations of the cutting blade (<3 μm peak-to-peak as measured with a photodiode device), which reduced damage to superficial structures in the slice. Slices were kept submerged in a maintenance chamber filled with sucrose-containing physiological saline at 35°C for 30 min after cutting and at 22°C during subsequent storage. Slices were then transferred into a recording chamber, where they were superfused with physiological saline at 34°C ± 2°C. MFBs in the stratum lucidum were visualized by infrared differential interference contrast (IR-DIC) videomicroscopy using a Zeiss axioscope equipped with a 60× Olympus water-immersion objective (numerical aperture 0.9, working distance 2 mm). In the process of development of the technique, the improvement of slicer mechanics, the use of sucrose-containing solution, and the availability of commercial high-numerical aperture objectives appeared to be key factors; details will be described elsewhere (J. R. P. Geiger, J. Bischofberger, U. Fröbe, S. Pfitzinger, H. J. Weber, K. Haverkampf, and P. Jonas, unpublished data).

Patch-Clamp Recording

Patch pipettes were pulled from borosilicate glass tubing (outer diameter, 2 mm; wall thickness, 0.7 mm for presynaptic recordings and 0.5 mm for postsynaptic recordings). When filled with internal solution, they had resistances of 5–12 MΩ (presynaptic pipettes) and 2–5 MΩ (postsynaptic pipettes). MFBs in the CA3c subfield were approached with positive pressure (80–130 mbar). In the presynaptic recordings analyzed, the seal resistance was >5 GΩ and the resting potential was -60 to -85 mV.

Axopatch 200A amplifiers (Axon Instruments, including circuits for series resistance compensation in the current-clamp mode) were used for current-clamp (I fast) and voltage-clamp recording. Holding potential was -80 mV in presynaptic whole-cell recordings, -90 mV in patch experiments, and -50 to -70 mV in postsynaptic whole-cell recordings, unless specified differently. Series resistance was <70 MΩ in presynaptic current-clamp recordings, <25 MΩ in presynaptic voltage-clamp recordings, and 5–20 MΩ in postsynaptic voltage-clamp recordings. Series resistance compensation was en-

abled (90% correction, 10–20 μs lag for presynaptic voltage-clamp experiments). Signals were filtered at 5 kHz (patch experiments) or 10 kHz (whole-cell recordings) with the low-pass Bessel filter of the amplifier or an external 8-pole Bessel filter (Frequency Devices, Haverhill, MA) unless specified differently. Filtered signals were digitized at 10–40 kHz using a 1401plus interface (with 16-bit DA/AD converters; Cambridge Electronic Design, UK). Pulse protocols were generated at a frequency of ≤0.5 Hz using homemade software. Leak and capacitive currents were subtracted using a P/−4 procedure. Patches with slowly rising outward currents and unusually large tail currents (presumably indicating K^+ depletion in partial vesicles) were excluded from analysis.

Paired Recordings

Paired recordings were made from a CA3 pyramidal neuron and an MFB attached directly to one of its primary apical dendrites. Due to rundown in the amplitude, recording of evoked EPSPs or EPSCs was limited to a time interval of ~5 min. In experiments with pre- and postsynaptic voltage-clamp (Figures 8B–8D), 2–5 complete runs, with increasing action potential duration in each run, were applied, and Ca^{2+} currents and EPSCs were averaged across trials. This protocol was chosen to minimize the consequences of rundown and to avoid an overestimation of the effects of action potential duration on EPSC amplitude. The large amplitude of the EPSCs (Figure 8) and the absence of paired-pulse facilitation (data not shown), which typically characterizes transmission at this synapse (Salin et al., 1996), suggests that the release probability is higher than under physiological conditions. This is probably due to the massive depolarization of the terminal during the approach with the patch pipette (leading to an induction of PTP and LTP) and the composition of the intracellular solution in the presynaptic pipette (internal GTP, phosphocreatine).

Staining

MFBs were filled with 0.5% biocytin (Molecular Probes) in K-gluconate or K-methylsulfate solution during recording. After withdrawal of the pipette, slices were kept for further 30 min in the recording chamber to allow for sufficient transport of the tracer. Slices were fixed in 100 mM phosphate buffer (pH 7.4) containing 4% paraformaldehyde (12 hr, 4°C) and were stained with fluorescein- or rhodamine-conjugated avidin (Vector Laboratories, 1: 200). After washing and mounting in Mowiol (Hoechst) or Prolong Antifade (Molecular Probes), MFBs were examined using epifluorescence illumination.

Analysis

Action potentials, patch currents, and EPSCs were analyzed using programs written in Pascal. Amplitude and duration at half-maximal amplitude of the action potential and the afterdepolarization following the spike were measured from the membrane potential preceding the stimulus, unless specified differently. Integrals were determined using Simpson's rule. The K^+ channel activation curve was obtained by calculating chord conductance values (G) from peak currents, assuming ohmic behavior and a reversal potential of −109 mV, and was fitted by a Boltzmann function raised to the fourth power. The inactivation curve was fitted with a simple Boltzmann function ($f = \{1 + \exp[(V - V_{1/2})/k]\}^{-1}$, where V is the membrane potential, $V_{1/2}$ the potential where f is 0.5, and k the slope factor).

Synaptic events were analyzed as described previously (Geiger et al., 1997). The rise time was determined as the time interval between the points corresponding to 20% and 80% of the peak amplitude, respectively. The peak current was determined as the maximum within a 2 ms window following the presynaptic action potential. The synaptic delay was determined as the time interval between the maximum of the first derivative of the presynaptic action potential and the onset of the average EPSC; the onset point was determined from the intersection of a line through the 20% and 80% points with the preceding baseline.

Membrane potentials are given without correction for liquid junction potentials. Values indicate mean ± SEM. Error bars in figures represent SEM when exceeding symbol size. Significance of differences was assessed by a two-tailed t test.

Solutions

Slices were superfused with physiological extracellular solution that contained 125 mM NaCl, 25 mM $NaHCO_3$, 25 mM glucose, 2.5 mM KCl, 1.25 mM NaH_2PO_4, 2 mM $CaCl_2$, and 1 mM $MgCl_2$ (bubbled with 95% O_2/5% CO_2 gas mixture). For dissection and storage of slices, a sucrose-containing physiological saline with 87 mM NaCl, 25 mM $NaHCO_3$, 25 mM glucose, 75 mM sucrose, 2.5 mM KCl, 1.25 mM NaH_2PO_4, 0.5 mM $CaCl_2$, and 7 mM $MgCl_2$ was used. For recording of presynaptic Ca^{2+} currents, 20 mM tetraethylammonium (TEA) Cl replaced equivalent amounts of NaCl and 1 μM TTX was added.

KCl and K-methylsulfate intracellular solutions (for presynaptic current-clamp and outside-out patch recordings) contained either 125 mM KCl or 110 mM K-methylsulfate plus 15 mM KCl, 4 mM $MgCl_2$, 4 mM K_2ATP, 0.5 mM Na_2GTP, 10 mM Na_2 phosphocreatine, 10 mM EGTA, and 10 mM HEPES. CsCl intracellular solution (for presynaptic whole-cell voltage-clamp recordings; Figure 7A) contained 145 mM CsCl, 2 mM $MgCl_2$, 2 mM Na_2ATP, 0.5 mM Na_2GTP, 5 mM Na_2 phosphocreatine, 10 mM EGTA, and 10 mM HEPES. K-gluconate internal solution (for intracellular staining; Figure 1) contained 120 mM K-gluconate, 20 mM KCl, 2 mM $MgCl_2$, 2 mM Na_2ATP, 10 mM EGTA, and 10 mM HEPES. K-methylsulfate intracellular solution (for presynaptic current-clamp recordings in pairs, Figure 8A) contained 125 mM K-methylsulfate, 12 mM KCl, 4 mM $MgCl_2$, 4 mM K_2ATP, 0.5 mM Na_2GTP, 5 mM Na_2 phosphocreatine, 50 μM BAPTA, and 10 mM HEPES. CsCl intracellular solution (for presynaptic voltage-clamp recordings in pairs; Figures 7B and 8B–8D) contained 160 mM CsCl, 2 mM $MgCl_2$, 2 mM Na_2ATP, 0.1 mM Na_2GTP, 5 mM Na_2 phosphocreatine, 50 μM BAPTA, and 10 mM HEPES. K-methylsulfate intracellular solutions (for postsynaptic voltage-clamp recordings in pairs) contained 110 mM K-methylsulfate plus 20 mM KCl, 2 mM $MgCl_2$, 2 mM Na_2ATP, 5 mM Na_2 phosphocreatine, 10 mM EGTA, and 10 mM HEPES. The pH of all internal solutions was adjusted to 7.3 with KOH or CsOH, respectively. Solutions for backfilling in outside-out patch experiments contained 100 U ml^{-1} creatine phosphokinase (which appeared to stabilize K^+ channel inactivation).

Blockers were applied either via bath perfusion or puffer application to outside-out patches. The application pipette solution contained 140 mM NaCl, 2.5 mM KCl, 1.8 mM $CaCl_2$, 1 mM $MgCl_2$, 5 mM HEPES, pH adjusted to 7.3 with NaOH; 0.1% bovine serum albumin was added in experiments with α-dendrotoxin (DTX). TTX was from Molecular Probes, DTX from Alomone (Jerusalem, Israel), K-methylsulfate from ICN; other chemicals were from Merck, Sigma, Riedel-de-Haën, or Gerbu.

Acknowledgments

We thank N. Spruston for his contribution to initial experiments. We also thank J. Bischofberger, M. Martina, and N. Spruston for critically reading an earlier version of the manuscript, and A. Blomenkamp for technical assistance. Supported by Deutsche Forschungsgemeinschaft (SFB 505/C5) and Human Frontiers Science Program Organization (RG-0017/98).

Received June 6, 2000; revised November 3, 2000.

References

Acsády, L., Kamondi, A., Sík, A., Freund, T., and Buzsáki, G. (1998). GABAergic cells are the major postsynaptic targets of mossy fibers in the rat hippocampus. J. Neurosci. *18*, 3386–3403.

Aldrich, R.W., Getting, P.A., and Thompson, S.H. (1979). Mechanism of frequency-dependent broadening of molluscan neurone soma spikes. J. Physiol. Lond. *291*, 531–544.

Amaral, D.G., and Dent, J.A. (1981). Development of the mossy fibers of the dentate gyrus: I. A light and electron microscopic study of the mossy fibers and their expansions. J. Comp. Neurol. *195*, 51–86.

Augustine, G.J. (1990). Regulation of transmitter release at the squid giant synapse by presynaptic delayed rectifier potassium current. J. Physiol. Lond. *431*, 343–364.

Bischofberger, J., and Jonas, P. (1997). Action potential propagation

into the presynaptic dendrites of rat mitral cells. J. Physiol. Lond. *504*, 359–365.

Blackstad, T.W., and Kjaerheim, Å. (1961). Special axo-dendritic synapses in the hippocampal cortex: electron and light microscopic studies on the layer of mossy fibers. J. Comp. Neurol. *117*, 133–146.

Borst, J.G.G., Helmchen, F., and Sakmann, B. (1995). Pre- and postsynaptic whole-cell recordings in the medial nucleus of the trapezoid body of the rat. J. Physiol. Lond. *489*, 825–840.

Borst, J.G.G., and Sakmann, B. (1999). Effect of changes in action potential shape on calcium currents and transmitter release in a calyx-type synapse of the rat auditory brainstem. Phil. Trans. R. Soc. Lond. B *354*, 347–355.

Brown, T.H., and Johnston, D. (1983). Voltage-clamp analysis of mossy fiber synaptic input to hippocampal neurons. J. Neurophysiol. *50*, 487–507.

Byrne, J.H., and Kandel, E.R. (1996). Presynaptic facilitation revisited: state and time dependence. J. Neurosci. *16*, 425–435.

Chandy, K.G., and Gutman, G.A. (1995). Voltage-gated potassium channel genes. In Ligand- and Voltage-Gated Ion Channels, Handbook of Receptors and Channels, R.A. North, ed. (Boca Raton, FL: CRC), pp. 1–71.

Cooper, E.C., Milroy, A., Jan, Y.N., Jan, L.Y., and Lowenstein, D.H. (1998). Presynaptic localization of Kv1.4-containing A-type potassium channels near excitatory synapses in the hippocampus. J. Neurosci. *18*, 965–974.

Derrick, B.E., and Martinez, J.L. (1994). Frequency-dependent associative long-term potentiation at the hippocampal mossy fiber-CA3 synapse. Proc. Natl. Acad. Sci. USA *91*, 10290–10294.

Drain, P., Dubin, A.E., and Aldrich, R.W. (1994). Regulation of *Shaker* K^+ channel inactivation gating by the cAMP-dependent protein kinase. Neuron *12*, 1097–1109.

Forsythe, I.D. (1994). Direct patch recording from identified presynaptic terminals mediating glutamatergic EPSCs in the rat CNS, *in vitro*. J. Physiol. Lond. *479*, 381–387.

Forsythe, I.D., Tsujimoto, T., Barnes-Davies, M., Cuttle, M.F., and Takahashi, T. (1998). Inactivation of presynaptic calcium current contributes to synaptic depression at a fast central synapse. Neuron *20*, 797–807.

Geiger, J.R.P., Lübke, J., Roth, A., Frotscher, M., and Jonas, P. (1997). Submillisecond AMPA receptor-mediated signaling at a principal neuron-interneuron synapse. Neuron *18*, 1009–1023.

von Gersdorff, H., and Matthews, G. (1994). Dynamics of synaptic vesicle fusion and membrane retrieval in synaptic terminals. Nature *367*, 735–739.

Griffith, W.H. (1990). Voltage-clamp analysis of posttetanic potentiation of the mossy fiber to CA3 synapse in hippocampus. J. Neurophysiol. *63*, 491–501.

Hopkins, W.F., and Johnston, D. (1984). Frequency-dependent noradrenergic modulation of long-term potentiation in the hippocampus. Science *226*, 350–352.

Jackson, M.B., Konnerth, A., and Augustine, G.J. (1991). Action potential broadening and frequency-dependent facilitation of calcium signals in pituitary nerve terminals. Proc. Natl. Acad. Sci. USA *88*, 380–384.

Johnston, D., Williams, S., Jaffe, D., and Gray, R. (1992). NMDA-receptor-independent long-term potentiation. Annu. Rev. Physiol. *54*, 489–505.

Jonas, P., Bräu, M.E., Hermsteiner, M., and Vogel, W. (1989). Single-channel recording in myelinated nerve fibers reveals one type of Na channel but different K channels. Proc. Natl. Acad. Sci. USA *86*, 7238–7242.

Jonas, P., Major, G., and Sakmann, B. (1993). Quantal components of unitary EPSCs at the mossy fibre synapse on CA3 pyramidal cells of rat hippocampus. J. Physiol. Lond. *472*, 615–663.

Jung, M.W., and McNaughton, B.L. (1993). Spatial selectivity of unit activity in the hippocampal granular layer. Hippocampus *3*, 165–182.

Llinás, R., Steinberg, I.Z., and Walton, K. (1981). Relationship between presynaptic calcium current and postsynaptic potential in squid giant synapse. Biophys. J. *33*, 323–352.

Ma, M., and Koester, J. (1996). The role of K^+ currents in frequency-dependent spike broadening in *Aplysia* R20 neurons: A dynamic-clamp analysis. J. Neurosci. *16*, 4089–4101.

Nicoll, R.A., and Malenka, R.C. (1995). Contrasting properties of two forms of long-term potentiation in the hippocampus. Nature *377*, 115–118.

Quattrocki, E.A., Marshall, J., and Kaczmarek, L.K. (1994). A *Shab* potassium channel contributes to action potential broadening in peptidergic neurons. Neuron *12*, 73–86.

Regehr, W.G., and Tank, D.W. (1991). The maintenance of LTP at hippocampal mossy fiber synapses is independent of sustained presynaptic calcium. Neuron *7*, 451–459.

Regehr, W.G., Delaney, K.R., and Tank, D.W. (1994). The role of presynaptic calcium in short-term enhancement at the hippocampal mossy fiber synapse. J. Neurosci. *14*, 523–537.

Rettig, J., Heinemann, S.H., Wunder, F., Lorra, C., Parcej, D.N., Dolly, J.O., and Pongs, O. (1994). Inactivation properties of voltage-gated K^+ channels altered by presence of β-subunit. Nature *369*, 289–294.

Rhodes, K.J., Strassle, B.W., Monaghan, M.M., Bekele-Arcuri, Z., Matos, M.F., and Trimmer, J.S. (1997). Association and colocalization of the Kvβ1 and Kvβ2 β-subunits with Kv1 α-subunits in mammalian brain K^+ channel complexes. J. Neurosci. *17*, 8246–8258.

Roeper, J., Sewing, S., Zhang, Y., Sommer, T., Wanner, S.G., and Pongs, O. (1998). NIP domain prevents N-type inactivation in voltage-gated potassium channels. Nature *391*, 390–393.

Ruppersberg, J.P., Schröter, K.H., Sakmann, B., Stocker, M., Sewing, S., and Pongs, O. (1990). Heteromultimeric channels formed by rat brain potassium-channel proteins. Nature *345*, 535–537.

Sabatini, B.L., and Regehr, W.G. (1999). Timing of synaptic transmission. Annu. Rev. Physiol. *61*, 521–542.

Salin, P.A., Scanziani, M., Malenka, R.C., and Nicoll, R.A. (1996). Distinct short-term plasticity at two excitatory synapses in the hippocampus. Proc. Natl. Acad. Sci. USA *93*, 13304–13309.

Schmitz, D., Frerking, M., and Nicoll, R.A. (2000). Synaptic activation of presynaptic kainate receptors on hippocampal mossy fiber synapses. Neuron *27*, 327–338.

Schneggenburger, R., Meyer, A.C., and Neher, E. (1999). Released fraction and total size of a pool of immediately available transmitter quanta at a calyx synapse. Neuron *23*, 399–409.

Sheng, M., Liao, Y.J., Jan, Y.N., and Jan, L.Y. (1993). Presynaptic A-current based on heteromultimeric K^+ channels detected *in vivo*. Nature *365*, 72–75.

Simmons, M.L., and Chavkin, C. (1996). κ-opioid receptor activation of a dendrotoxin-sensitive potassium channel mediates presynaptic inhibition of mossy fiber neurotransmitter release. Mol. Pharmacol. *50*, 80–85.

Skaggs, W.E., McNaughton, B.L., Wilson, M.A., and Barnes, C.A. (1996). Theta phase precession in hippocampal neuronal populations and the compression of temporal sequences. Hippocampus *6*, 149–172.

Southan, A.P., and Robertson, B. (1998). Patch-clamp recordings from cerebellar basket cell bodies and their presynaptic terminals reveal an asymmetric distribution of voltage-gated potassium channels. J. Neurosci. *18*, 948–955.

Spencer, A.N., Przysiezniak, J., Acosta-Urquidi, J., and Basarsky, T.A. (1989). Presynaptic spike broadening reduces junctional potential amplitude. Nature *340*, 636–638.

Spruston, N., Jonas, P., and Sakmann, B. (1995). Dendritic glutamate receptor channels in rat hippocampal CA3 and CA1 pyramidal neurons. J. Physiol. Lond. *482*, 325–352.

Spruston, N., Lübke, J., and Frotscher, M. (1997). Interneurons in the stratum lucidum of the rat hippocampus: an anatomical and electrophysiological characterization. J. Comp. Neurol. *385*, 427–440.

Stanley, E.F. (1991). Single calcium channels on a cholinergic presynaptic nerve terminal. Neuron *7*, 585–591.

Steinhäuser, C. (1993). Electrophysiologic characteristics of glial cells. Hippocampus *3*, 113–124.

Stühmer, W., Ruppersberg, J.P., Schröter, K.H., Sakmann, B., Stocker, M., Giese, K.P., Perschke, A., Baumann, A., and Pongs, O. (1989). Molecular basis of functional diversity of voltage-gated potassium channels in mammalian brain. EMBO J. *8*, 3235–3244.

Thorn, P.J., Wang, X., and Lemos, J.R. (1991). A fast, transient K^+ current in neurohypophysial nerve terminals of the rat. J. Physiol. Lond. *432*, 313–326.

Verhage, M., McMahon, H.T., Ghijsen, W.E.J.M., Boomsma, F., Scholten, G., Wiegant, V.M., and Nicholls, D.G. (1991). Differential release of amino acids, neuropeptides, and catecholamines from isolated nerve terminals. Neuron *6*, 517–524.

Villacres, E.C., Wong, S.T., Chavkin, C., and Storm, D.R. (1998). Type I adenylyl cyclase mutant mice have impaired mossy fiber long-term potentiation. J. Neurosci. *18*, 3186–3194.

Wang, H., Kunkel, D.D., Schwartzkroin, P.A., and Tempel, B.L. (1994). Localization of Kv1.1 and Kv1.2, two K channel proteins, to synaptic terminals, somata, and dendrites in the mouse brain. J. Neurosci. *14*, 4588–4599.

Wang, L.-Y., and Kaczmarek, L.K. (1998). High-frequency firing helps replenish the readily releasable pool of synaptic vesicles. Nature *394*, 384–388.

Weisskopf, M.G., Castillo, P.E., Zalutsky, R.A., and Nicoll, R.A. (1994). Mediation of hippocampal mossy fiber long-term potentiation by cyclic AMP. Science *265*, 1878–1882.

Wheeler, D.B., Randall, A., and Tsien, R.W. (1996). Changes in action potential duration alter reliance of excitatory synaptic transmission on multiple types of Ca^{2+} channels in rat hippocampus. J. Neurosci. *16*, 2226–2237.

Wiebe, S.P., and Stäubli, U.V. (1999). Dynamic filtering of recognition memory codes in the hippocampus. J. Neurosci. *19*, 10562–10574.

Yeckel, M.F., and Berger, T.W. (1998). Spatial distribution of potentiated synapses in hippocampus: Dependence on cellular mechanisms and network properties. J. Neurosci. *18*, 438–450.

Zalutsky, R.A., and Nicoll, R.A. (1990). Comparison of two forms of long-term potentiation in single hippocampal neurons. Science *248*, 1619–1624.